Electronic Structures of $M_{21}S_8$ (M = Nb, Zr) and $(M,M')_{21}S_8$ (M, M′ = Hf, Ti; Nb, Ta) Phases and Reasons for Variations in the Metal Site Occupations

Martin Köckerling*,† and Enric Canadell*,‡

FB6-Institut für Synthesechemie, Gerhard-Mercator-Universität, Lotharstrasse 1, 47057 Duisburg, Germany, and Institut de Ciència de Materials de Barcelona (CSIC), Campus de la UAB, 08193 Bellaterra, Spain

Received October 18, 1999

The electronic structures of binary $M_{21}S_8$ (M = Nb, Zr) and isostructural ternary $(M,M')_{21}S_8$ (M, M′ = Hf, Ti; Nb, Ta) phases have been studied by means of extended Hückel tight-binding band structure calculations. For the valence electron concentration in the binary group 5 metal phase $Nb_{21}S_8$, metal−metal bonding is optimized whereas, in the isostructural group 4 metal phase $Zr_{21}S_8$, metal−metal bonding levels exist above the Fermi level. However, the electronic structure analysis suggests a stable structure for $M_{21}S_8$ phases with group 4 metals and that $(M,M')_{21}S_8$ phases with mixed group 4 and group 5 metals, even if not yet reported, could well exist. In the ternary phase $Nb_{6.9}Ta_{14.1}S_8$, a linear relationship exists between the magnitude of the metal−metal bonding capacity (as expressed by the total metal−metal Mulliken overlap population) of each crystallographically independent metal site and the occupation of the site with the heavier metal (i.e., the element with the greater bonding capability). The situation is quite more complex in $Hf_{7.5}Ti_{13.5}S_8$, where the metal−metal bonding capacity of each site, differences in electronegativity between Ti and Hf, and site volume arguments must be taken into account to understand the metal site occupation.

Introduction

On the borderline of intermetallic alloys and ionic materials, chemical compounds have been discovered that exhibit unprecedented compositions and original structures as well as interesting physical properties. A large subgroup of these is found for the binary and ternary metal-rich sulfides of groups 3−6.[1−5] Compounds of this type are usually prepared by high-temperature techniques ($T > 1400$ K), and they are three-dimensionally tightly bonded systems stabilized by extensive arrays of metal−metal bonds. Previously unexpected structural features, named *differential site occupancies*, are found in some of these compounds, like the ternary Nb−Ta sulfides $Nb_{4.92}Ta_{6.08}S_4$ ($M_{11}S_4$),[6] $Nb_{6.74}Ta_{5.26}S_4$ ($M_{12}S_4$),[7] $Nb_{1.72}Ta_{3.28}S_2$ ($M_{10}S_4$),[8,9] and $Nb_{0.4}Ta_{1.6}S$ (M_8S_4),[10,11] which show three characteristic properties that set them apart as a subcategory of crystalline solids: (1) Each metal site is statistically (to X-rays) occupied by a mixture of the two metals. (2) The fractional occupancy of each site is rather narrowly fixed but varies substantially comparing the different sites. (3) The structures of the ternaries are not found for either of the corresponding binary systems.

A strongly related class of materials has the composition $M_{21}S_8$[12] and is known for ternaries $(M,M')_{21}S_8$ with M, M′ = Nb, Ta[13] and Hf, Ti[14] as well as for binaries with M = Zr[15] and Nb.[16,17] It is the existence of the two binaries (see point 3 above) which does not strictly allow us to consider these phases among those showing *differential site occupancies* although the ternaries share the first two points with them. The recently discovered superconductivity in $Nb_{21}S_8$[18] as well as some special structural features found in the ternaries makes the study of these phases very appealing.

Extended Hückel band structure calculations on the Nb−Ta sulfides have shown that the amount of the heavier element (i.e., the element with the greater bonding capability) on each site is linearly correlated with the metal−metal bonding capacity of the corresponding site as measured from the total metal−metal Mulliken overlap population.[1] Thus, the small differences in bonding capabilities between Nb and Ta give rise to the formation of materials that are unknown for each (or just one)

† Gerhard-Mercator-Universität.
‡ Institut de Ciència de Materials de Barcelona.

(1) Franzen, H. F.; Köckerling, M. *Prog. Solid State Chem.* **1995**, *23*, 265−289.
(2) Franzen, H. F. *Prog. Solid State Chem.* **1978**, *12*, 1−39.
(3) Hughbanks, T. *J. Alloys Compd.* **1995**, *229*, 40−53.
(4) Harbrecht, B.; Degen, Th.; Conrad, M. *J. Alloys Compd.* **1997**, *246*, 37−50.
(5) Tremel, W.; Kleinke, H.; Derstroff, V.; Reisner, C. *J. Alloys Compd.* **1995**, *219*, 73−82.
(6) Yao, X.; Franzen, H. F. *J. Solid State Chem.* **1990**, *86*, 88−93.
(7) Yao, X.; Franzen, H. F. *Z. Anorg. Allg. Chem.* **1991**, *598/599*, 353−362.
(8) Wang, Z.; Johnston, D. C.; Yao, X.; Franzen, H. F. *Physica C* **1995**, 138−140.
(9) Yao, X.; Franzen, H. F. *J. Am. Chem. Soc.* **1991**, *113*, 1426−1427.
(10) Yao, X.; Miller, G. J.; Franzen, H. F. *J. Alloys Compd.* **1992**, *183*, 7−17.
(11) Nanjundaswamy, K. S.; Hughbanks, T. *J. Solid State Chem.* **1992**, *98*, 278−290.
(12) Note that structural similarities with the $M_{21}S_8$ phases are found in the recently discovered $Zr_9Co_2P_4$ and $Zr_9Ni_2P_4$: Kleinke, H.; Franzen, H. F. *Inorg. Chem.* **1996**, *35*, 5272−5277.
(13) Yao, X.; Franzen, H. F. *J. Alloys Compd.* **1992**, *182*, 299−312.
(14) Harbrecht, B. *Z. Kristallogr.* **1989**, *186*, 119−120.
(15) Conard, B. R.; Franzen, H. F. *High Temp. Sci.* **1971**, *3*, 49−55.
(16) Franzen, H. F.; Beinecke, T. A.; Conard, B. R. *Acta Crystallogr.* **1968**, *B24*, 412−416.
(17) The existence of two more compounds with the $M_{21}S_8$ structure ($Mo_{21}S_8$ and $W_{21}S_8$) is briefly mentioned in the literature, but further investigations seem to be necessary to verify that these are in fact stoichiometric binary phases: Nanjundaswamy, K. S.; Gopalakrishnan, J. *J. Solid State Chem.* **1987**, *68*, 188−191.
(18) Köckerling, M.; Johrendt, D.; Finckh, E. W. *J. Am. Chem. Soc.* **1998**, *120*, 12297−12302.

10.1021/ic991218t CCC: $19.00
Published on Web 08/26/2000

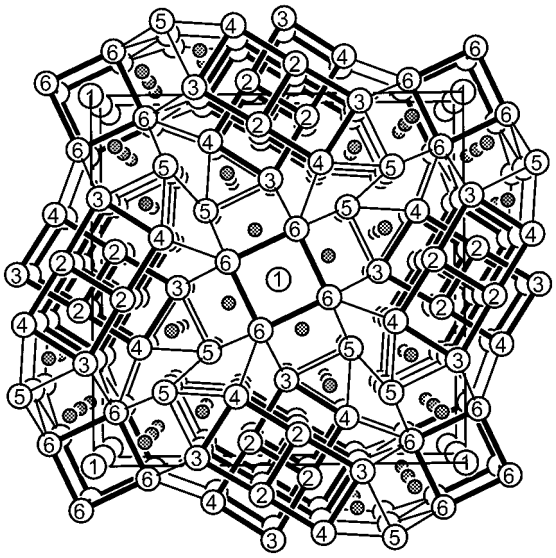

Figure 1. [001] view of the unit cell of $Nb_{21}S_8$: Nb, open circles with atom numbering; S, small shaded circles. The body-centered Nb cubes are emphasized.

Table 1. Structural Details for Each Member of the $M_{21}S_8$ Series of Compounds

compound	lattice params		unit cell vol (Å^3)	ref
	a (Å)	*c* (Å)		
$Zr_{21}S_8$	16.88(5)	3.42(1)	974(9)	15
$Nb_{21}S_8$	16.794(5)	3.359(2)	947(1)	16
$Nb_{6.9}Ta_{14.1}S_8$	16.817(2)	3.3450(9)	946.0(5)	13
$Hf_{7.5}Ti_{13.5}S_8$	16.970(4)	3.3618(4)	968.1(7)	14

of the binary systems, like the above-mentioned $Nb_{4.92}Ta_{6.08}S_4$,[6] a compound whose structure has not been realized (so far) for either $Ta_{11}S_4$ or $Nb_{11}S_4$ (see above for more examples). Intriguingly, this correlation seems to break down for the $(M,M')_{21}S_8$ type phase $Hf_{7.5}Ti_{13.5}S_8$. Here, the site with the highest total metal−metal overlap population does not have the highest amount of hafnium. It is also interesting to note that the same structure type exists for different valence electron concentrations (see ref 19) which range from 3.2 for $Zr_{21}S_8$ and $Hf_{7.5}Ti_{13.5}S_8$ to 4.2 for $Nb_{21}S_8$ and $Nb_{6.9}Ta_{14.1}S_8$. This situation prompts a thorough investigation of the electronic structures of this series of compounds as well as all possible electronic and structural factors that determine the amount of metal on each site in the ternary phases.

Here we report an extended Hückel tight-binding band structure study of the bonding in the $M_{21}S_8$ and $(M,M')_{21}S_8$ type phases to understand the metal site occupation in the ternary $Ti_{13.5}Hf_{7.5}S_8$ as well as the stability ranges for different valence electron counts.

Crystal Structure

The different members of the isostructural series $M_{21}S_8$ with M = Zr, Hf + Ti, Nb, and Nb + Ta crystallize in the tetragonal space group *I*4/*m* with the metallic substructure being built up from six crystallographically independent sites, M1 to M6, and two independent sulfur sites, S1 and S2. A projection of the structure along the *c* axis is shown in Figure 1. Important structural parameters are listed in Table 1. Structural details from single-crystal X-ray studies are reported for M = Nb, Nb + Ta, and Ti + Hf. Distances between atoms and site volumes are given in Table 2. The data for these phases, for which the lattice parameters were obtained from powder X-ray diffraction, were calculated using the atomic coordinates of $Nb_{21}S_8$ and the cell parameters of the corresponding phase.

Table 2. Atomic Environments of the Six Crystallographically Independent metal Sites in the $M_{21}S_8$ Phases

All $M_{21}S_8$ and $(M,M')_{21}S_8$ Phases

site	no. of M−M bonds	no. of M−S bonds	no. of atoms/unit cell
1	10	4	2
2	13	1	8
3	12	3	8
4	12	2	8
5	11	4	8
6	11	4	8

$Zr_{21}S_8$

site	shortest M−M bond (Å)	av M−M bond (Å)	av M−S bond (Å)	site vol[31] (Å^3)
1	2.976	3.065	2.561	54.1
2	2.876	3.078	2.622	69.4
3	2.932	3.234	2.556	77.1
4	2.902	3.116	2.507	71.0
5	2.902	3.236	2.608	71.1
6	2.976	3.230	2.568	76.6

$Nb_{6.9}Ta_{14.1}S_8$

site	shortest M−M bond (Å)	av M−M bond (Å)	av M−S bond (Å)	site vol (Å^3)
1	2.947	3.027	2.551	52.5
2	2.847	3.045	2.612	67.4
3	2.903	3.203	2.533	74.9
4	2.873	3.085	2.477	68.9
5	2.873	3.203	2.588	69.1
6	2.947	3.197	2.538	71.4

$Nb_{21}S_8$

site	shortest M−M bond (Å)	av M−M bond (Å)	av M−S bond (Å)	site vol (Å^3)
1	2.949	3.031	2.548	52.6
2	2.849	3.047	2.609	67.5
3	2.904	3.204	2.534	74.9
4	2.875	3.087	2.480	69.0
5	2.875	3.205	2.588	69.2
6	2.949	3.199	2.541	71.5

$Hf_{7.5}Ti_{13.5}S_8$[a]

site	shortest M−M bond (Å)	av M−M bond (Å)	av M−S bond (Å)	site vol (Å^3)
1	3.004	3.076	2.540	55.6
2	2.824	3.053	2.658	67.8
3	2.851	3.234	2.587	76.5
4	2.851	3.105	2.542	70.0
5	2.911	3.242	2.572	69.8
6	3.004	3.230	2.566	74.5

[a] For comparison: elemental hafnium (hcp, α-Hf, 12-coordinate) average M−M 3.161 Å, site volume 74.4 Å^3; elemental titanium (hcp, α-Ti, 12-coordinate) average M−M 2.923 Å, site volume 58.8 Å^3.

The main feature of the $M_{21}S_8$ structure is an extended network of metal−metal bonds. Two different types of condensed metal cluster chains run along [001] in the tetragonal structure. Both cluster chain types consist of body-centered niobium cubes condensed via opposite faces. The first type is just a single chain of cubes that are centered at the edges and the centers of the unit cell. The smaller unit of the second type consists of two double cubes, one being rotated 90° relative to the other, giving a starlike arrangement. Thereby the niobium atoms in the centers of the first double-cube chain are at the corners of the second double chain. These two types of "metal-

(19) Simon, A. *Angew. Chem.* **1988**, *100*, 164−188.

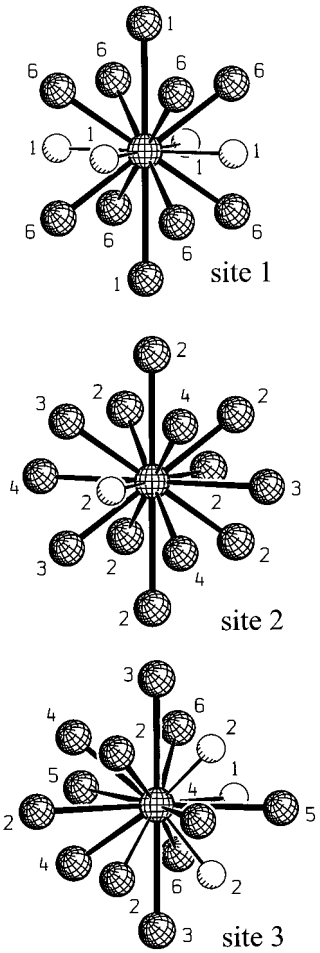

Figure 2. Coordination environments of the Nb1, Nb2, and Nb3 sites in $Nb_{21}S_8$ up to distances of 4.0 Å, with atom numbering: Nb, hatched circles; S, open circles.

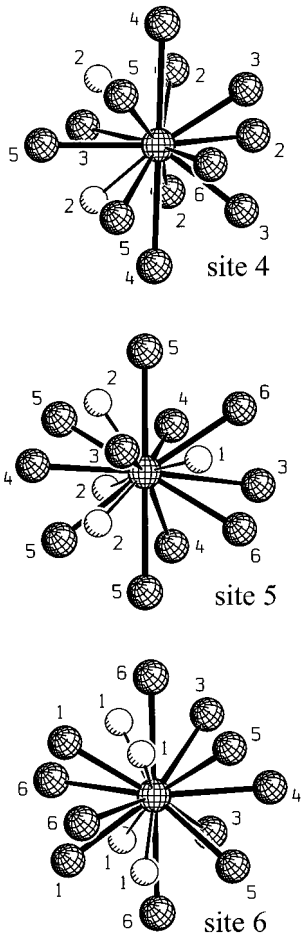

Figure 3. Coordination environments of the Nb4, Nb5, and Nb6 sites in $Nb_{21}S_8$ up to distances of 4.0 Å, with atom numbering: Nb, hatched circles; S, open circles.

tubing", as highlighted in Figure 1, show the close relationship of these sulfides to the elements. From a different viewpoint, the metal atom arrangement can be described as consisting of compressed and fused M_6 octahedra. This description allows for comparison with other metal-rich early transition element compounds.[19]

The atomic environments of the six crystallographically independent metal sites (see Figure 1) differ largely from site to site. The coordination polyhedra of each of these up to distances of 4.0 Å are depicted in Figures 2 and 3. Table 2 gives all structurally relevant parameters for each site.

Electronic Structure

A. Computational Details. The electronic structures of the $M_{21}S_8$ and $(M,M')_{21}S_8$ phases were calculated by means of the extended Hückel tight-binding method[20,21] using the EHMACC program, adapted to an IBM-compatible PC.[22] The calculations were carried out using a mesh of 27 K points, evenly spread throughout the asymmetric parts of the unit cells, which were reduced from the body-centered to the primitive setting. The valence shell ionization potentials,[23] Slater type orbital exponents, and contraction coefficients for the double-ζ type orbitals employed in the calculations are summarized in Table 3.

To check the effect of different atomic orbital parameters on our final conclusions, we performed several further series of calculations employing a variety of different parameters. It was found that the chemically important conclusions, as outlined in the following sections, were not altered. Therefore, the parameters in Table 3, which were taken from the literature, were employed. Total Mulliken overlap population quantities (TMOP) were calculated which take into account all overlap populations between a metal atom M and all surrounding metal neighbors M′ up to distances of 4.0 Å.[28]

B. Electronic Structure of the $M_{21}S_8$ Phases. The band structure of the $M_{21}S_8$ phases (see ref 18 for a study of $Nb_{21}S_8$) is rather complicated because of the size of the unit cell and the complexity of the system. Therefore, in the present work,

(20) Whangbo, M.-H.; Hoffmann, R. *J. Am. Chem. Soc*. **1978**, *100*, 6093−6098.
(21) A modified Wolfsberg−Helmholz formula (Ammeter, J. H.; Bürgi, H.-B.; Thibeault, J. C.; Hoffmann, R. *J. Am. Chem. Soc*. **1978**, *100*, 3686−3692) was used to evaluate the off-diagonal $H_{\mu\nu}$ values.
(22) Whangbo, M.-H.; Hoffmann, R.; Hughbanks, T.; Kertesz, M.; Wijeyesekera, S.; Wilker, C.; Zheng, C.; Evain, M. *EHMACC: A Program for Extended Hückel Molecular and Crystal Calculations*; Departments of Chemistry, Cornell University, Ithaca, NY and North Carolina State University, Raleigh, NC, 1987. PC adaptation: M. Köckerling, Institut für Synthesechemie, University of Duisburg, 1996.
(23) Vela, A.; Gázquez, J. L. *J. Phys. Chem.* **1988**, *92*, 5688−5693.
(24) Saillard, J.-Y.; Hoffmann, R. *J. Am. Chem. Soc.* **1984**, *106*, 2006−2026.
(25) Tatsumi, K.; Nakamura, A.; Hofmann, P.; Stauffert, P.; Hoffmann, R. *J. Am. Chem. Soc*. **1985**, *107*, 4440−4451.
(26) Hoffman, D. M.; Hoffmann, R.; Fisel, C. R. *J. Am. Chem. Soc*. **1982**, *104*, 3858−3875.
(27) Abdon, R. L.; Hughbanks, T. *J. Am. Chem. Soc*. **1995**, *117*, 10035−10040.
(28) Burdett, J. K. *Chemical Bonding in Solids*; Oxford University Press: New York, 1995; p 6.

Table 3. Valence Shell Ionization Potentials (H_{ii}), Exponents (ζ_i) of the Slater-Type Orbitals (χ_i), and Contraction Coefficients Used in the Double-ζ Type Expansions for the Extended Hückel Tight-Binding Calculations

atom	χ_i	H_{ii}[23] (eV)	$\zeta 1_i$[a]	c_1[b]	$\zeta 2_i$[a]	c_2[b]
Ti[24]	4s	−6.520	1.500			
	4p	−3.808	1.500			
	3d	−7.177	4.550	0.4206	1.400	0.7839
Zr[25]	5s	−6.410	1.817			
	5p	−3.774	1.776			
	4d	−6.969	3.835	0.6210	1.505	0.5769
Nb[11,26]	5s	−6.705	1.890			
	5p	−3.878	1.850			
	4d	−8.144	4.080	0.6401	1.640	0.5516
Hf[27]	6s	−6.606	2.210			
	6p	−3.838	2.170			
	5d	−6.895	4.360	0.6967	1.709	0.5322
Ta[11,26]	6s	−6.889	2.280			
	6p	−3.939	2.241			
	5d	−8.028	4.762	0.6106	1.938	0.6106
S[26]	3s	−20.000	2.122			
	3p	−13.300	1.827			

[a] Slater-type orbital exponents. [b] Contraction coefficients used in the double-ζ type orbitals.

results are presented in a more straightforward fashion using density of states (DOS) and crystal orbital overlap population (COOP) curves. Those for $Nb_{21}S_8$ are shown in Figure 4. In the DOS curve, the sulfur contributions are shaded. The Fermi level at −7.82 eV (marked A in Figure 4 for $Nb_{21}S_8$) cuts through a small local maximum inside a deep minimum in a region that covers predominantly Nb states. Interestingly, this DOS curve resembles very closely the curve that was obtained by the TB-LMTO-ASA method.[18] The Fermi level for the isostructural but electron poorer compound $Zr_{21}S_8$ is marked in Figure 4 as a line labeled B. COOP curves in Figure 4 are given for all metal−metal interactions as well as for all metal−sulfur interactions up to distances of 4.0 Å.

The mainly niobium- and sulfur-based states are clearly separated by a gap of about 1.5 eV. Of course, there is some sulfur contribution in the mostly metal-based DOS above the gap, which corresponds to the metal−sulfur antibonding interactions. However, it is spread out over a wide energy range. This leads to very small changes in the sulfur contribution and consequently in the metal−sulfur overlap population when the Fermi level is lowered to the value appropriate for the group 4 metal phases. Consequently, it is anticipated that the metal−sulfur contributions should not provide any differential effect when the group 4 and group 5 $M_{21}S_8$ and $(M,M')_{21}S_8$ phases are compared. It is clear from the DOS in Figure 4 that the sulfurs can be considered as S^{2-}. As shown in Figure 4, the metal−metal bonding is optimized for the electron count of the group 5 metal phases. The metal−sulfur interactions are slightly antibonding around the Fermi level, but as expected, these contributions are very small and are overwhelmed by the magnitude of the metal−metal bonding interactions. For the group 4 metals, the metal−metal bonding is not optimized as much as that for the group 5 metal containing compounds.

Since the Fermi level cuts through a region that is predominantly metal in character, before proceeding to a more careful analysis of the bonding capabilities of each site and, more importantly, to a comparison of the results for the group 4 and group 5 phases, it is important to see if a rigid-band scheme works well for these compounds. The calculated DOS and COOP curves for $Zr_{21}S_8$ are shown in Figure 5. Comparison of these results with those of Figure 4 suggests that this assumption is valid indeed.

The numerical values of the total Mulliken overlap populations (TMOP's), which represent the strengths of the metal−metal and metal−sulfur interactions for each metal site of $Nb_{21}S_8$, as well as for the hypothetical phases $Hf_{21}S_8$ and $Ti_{21}S_8$ (calculated using the structural parameters of $Hf_{7.5}Ti_{13.5}S_8$), are given in Table 4. Calculations on the hypothetical phases $Hf_{21}S_8$ and $Ti_{21}S_8$, which have so far not been shown to exist, were chosen as models for $Hf_{7.5}Ti_{13.5}S_8$ because an appropriate modeling of the fractional occupation of the metal sites implicates the use of larger unit cells, something which obviously cannot be handled for such a complex compound. From the data in Table 4, it is clear that the total metal−metal Mulliken overlap populations vary substantially from site to site for either phase.[1] Note that these results can only be partially understood from purely structural arguments—for instance, taking into account the number and average value of the M−M bonds for each site—so that orbital interaction effects, which can only be quantified through the overlap populations, must play a nonnegligible role.

One of the interesting results of Table 4 is that when the magnitude of the metal−metal bonding in $Nb_{21}S_8$ is compared with that of either $Ti_{21}S_8$ or $Hf_{21}S_8$, the latter phases are found to exhibit stronger bonding. Of course, it is difficult to compare overlap populations calculated for different atoms because these quantities can be affected by the parameters used in the calculations (i.e., the orbital exponents). However, we note that the same result was found for all atoms of group 4 whatever their size (recall that calculations were also carried out for $Zr_{21}S_8$) and that the parameter sets for the transition metal atoms come from different sources (also, as noted in section A, this observation was found to hold when we carried out several check calculations changing the parameters). It seems that the loss of metal−metal bonding on going from the group 5 to the group 4 metal phases, which have less than the optimal electron counts for metal−metal bonding, seems to be compensated by stronger bonds. The reason probably lies in the intrinsic differences between the d orbitals of group 4 and group 5 metals and the very similar average metal−metal bond distances for the $M_{21}S_8$ and $(M,M')_{21}S_8$ phases (see Table 2), which lead to the dominance of the metal−metal overlap interactions for the group 4 metals, whatever the atom is, over those of the group 5 metals. At the first sight, the stronger metal−metal bonding in the group 4 compared to the group 5 sulfides is surprising in view of the higher melting point of elemental Nb (2468 °C) compared to that of elemental Zr (1852 °C). To ensure that this result is real and does not reflect incorrectly chosen AO parameters, metal−metal TMOP's were calculated for both of these elements. The larger value for Nb, which is perfectly consistent with its known physical properties, compared to the value for Zr confirms the interesting though unexpected result of stronger metal−metal bonding in the group 4 metal-rich sulfides. This suggests also that there should be a range of valence electron concentrations compatible with this type of structure. The stability of the structure for electron counts appropriate for group 4 and 5 metals leads to the idea that this structure could also be stable when M and M′ are group 4 and group 5 metal atoms, respectively. In view of the recent observation of superconductivity in $Nb_{21}S_8$, it would be very interesting to carry out physical measurements on this type of phase to analyze the influence of valence electron concentrations and disorder on superconductivity in phases with extensive metal−metal bonding.

Comparing the TMOP's for the metal−sulfur interactions (lower part of Table 4), we find out that, for each site, they

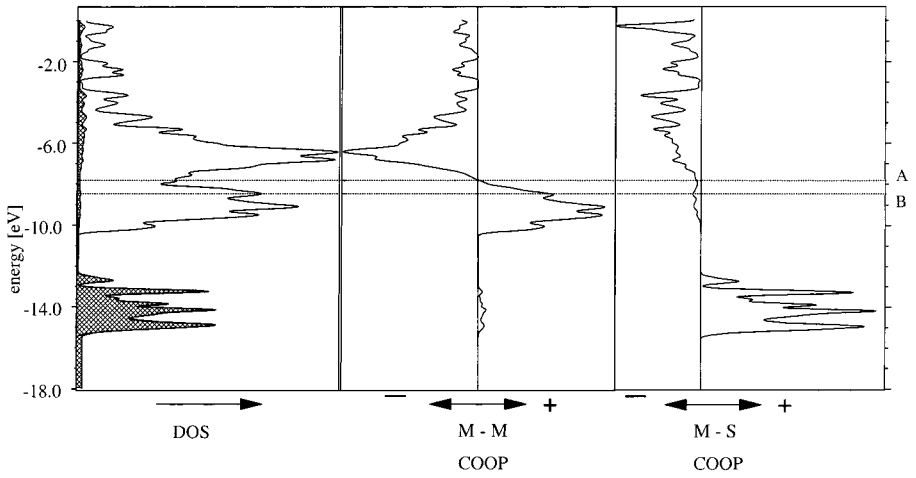

Figure 4. Density of states (DOS) curves (left part), with the sulfur contributions shaded, and crystal orbital overlap population (COOP) curves for all metal−metal and metal−sulfur interactions up to 4.0 Å in $Nb_{21}S_8$. Fermi levels are marked by horizontal lines for $Nb_{21}S_8$ (A) and $Zr_{21}S_8$ (B).

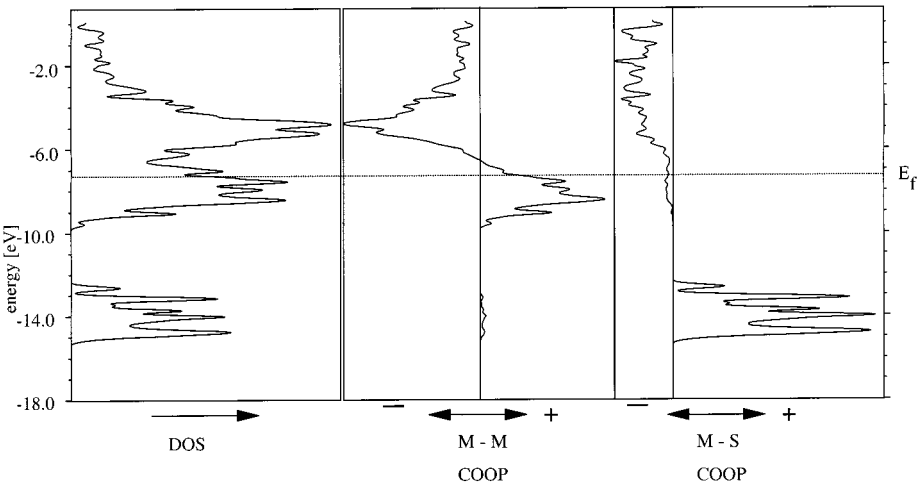

Figure 5. Density of states (DOS) curves (left part) and crystal orbital overlap population (COOP) curves for all metal−metal and metal−sulfur interactions up to 4.0 Å in $Zr_{21}S_8$. The Fermi level is marked by a horizontal line.

Table 4. Total Mulliken Overlap Populations for All Metal−Metal and Metal−Sulfur Interactions up to 4.0 Å for the Six Different Metal Sites in the $M_{21}S_8$ Phases

site	no. of bonds	TMOP's $Ti_{21}S_8$	$Hf_{21}S_8$	$Nb_{21}S_8$
		Metal−Metal Interactions		
1	10	1.71	1.86	1.69
2	13	3.46	3.52	3.08
3	12	2.33	2.43	2.05
4	12	2.79	2.90	2.49
5	11	1.74	1.82	1.68
6	11	1.62	1.69	1.53
		Metal−Sulfur Interactions		
1	4	1.01	1.01	0.95
2	1	0.18	0.17	0.17
3	3	0.81	0.81	0.86
4	2	0.55	0.55	0.59
5	4	1.11	1.10	1.04
6	4	1.13	1.12	1.12

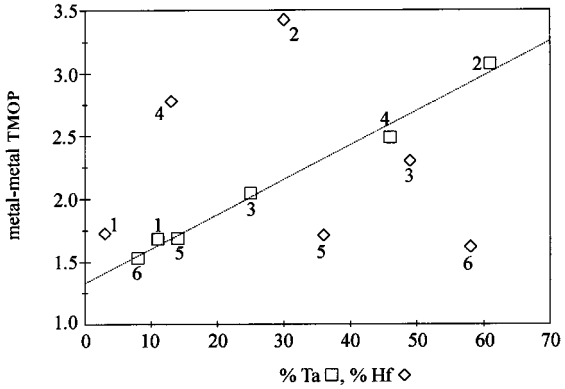

Figure 6. Total metal−metal Mulliken overlap populations (TMOP's) for metal sites in $Nb_{21}S_8$ vs % Ta occupation in $Nb_{6.9}Ta_{14.1}S_8$ (squares) and TMOP's for metal sites in $Ti_{21}S_8$ vs % Hf occupation in $Hf_{7.5}Ti_{13.5}S_8$ (rhombuses).

differ only marginally on going from one phase to the other. This is consistent with our analysis of the sulfur projected DOS curve. Thus, from these numbers, we can draw the important conclusion that structural differences or differences in the occupation of the metal sites between the phases do not arise from differences in the metal−sulfur bonding capabilities.

C. The Site Occupation Problem in the $(M,M')_{21}S_8$ Phases. As mentioned in the Introduction, the occupations of the six crystallographically independent metal sites in the ternary phase $Hf_{7.5}Ti_{13.5}S_8$ differ largely from what could be expected on the basis of the previous analysis of $Nb_{6.9}Ta_{14.1}S_8$. In this phase, the amount of the heavier element varies linearly with the metal−metal TMOP on each site.[1] This situation is graphically presented in Figure 6. The linear relation can be rationalized on the basis of the very similar sizes (1.46 Å)[29] and comparable electronegativities of the niobium and tantalum atoms. Differ-

Table 5. Occupation of the Six Metal Sites in $Nb_{6.9}Ta_{14.1}S_8$ and $Hf_{7.5}Ti_{13.5}S_8$ by the Heavier Elements and Average Charges on the Metal Sites in (Hypothetical) "$Hf_{21}S_8$" and "$Ti_{21}S_8$"

site	% Ta in $Nb_{6.9}Ta_{14.1}S_8$	% Hf in $Hf_{7.5}Ti_{13.5}S_8$	av charges on metal sites	
			$Hf_{21}S_8$	$Ti_{21}S_8$
1	14	3	+0.31	+0.44
2	61	30	−0.64	−0.70
3	25	49	+0.23	+0.24
4	46	13	−0.09	−0.15
5	11	36	+0.63	+0.66
6	8	58	+0.74	+0.71

ences in bonding properties should arise only from the fact that the sixth-row element Ta has more diffuse orbitals, which assemble better metal−metal bonding. Also included in Figure 6 is the percent Hf occupation on each site in $Ti_{13.5}Hf_{7.5}S_8$ versus the TMOP for each site in $Ti_{21}S_8$ (the same type of figure is obtained when results for $Hf_{21}S_8$ or $Zr_{21}S_8$ are used). These values do not follow a simple trend at all. Clearly, despite the fact that metal−metal interactions seem to dominate the bonding in these phases, factors other than the metal−metal TMOP need to be considered. The more likely ones are differences between Hf and Ti (1) in the metal−sulfur bonding, (2) in electronegativity, and (3) in size.

Sites 1, 2, and 4 are occupied by more Ti (less Hf) and sites 3, 5, and 6 are occupied by more Hf (less Ti) than would be expected on the basis of TMOP's. As discussed above, the metal−sulfur interactions do not vary no matter which metal parameters (for Ti, Hf, or Nb) are used. Thus, they are not responsible for the observed distributions of Hf and Ti on the metal sites in $Hf_{7.5}Ti_{13.5}S_8$.

More important is the difference in electronegativity between Hf (Pearson's absolute electronegativity:[30] 2.95) and Ti (3.45). The more electronegative Ti should prefer the sites with the higher negative charges. The average charges on the metal sites, as calculated for both the hypothetical $Hf_{21}S_8$ and $Ti_{21}S_8$ phases, are listed in Table 5, together with the percentage occupations of the sites by the heavier element in each case. Sites 2 and 4 appear to have accumulated the highest negative charges. This corresponds nicely with the fact that these sites have accumulated much higher amounts of titanium than would be expected from the metal−metal TMOP argument. In Figure 6, these two entries are moved to the left of the TMOP line. The other four sites carry positive charges; thus they prefer to accumulate larger amounts of the more electropositive hafnium. This argument fits for sites 3, 5, and 6, even semiquantitatively, since the higher the positive charge, the more the site occupation differs from the values expected on the basis of the TMOP argument. In Figure 6, these entries are located to the right of the ideal metal−metal TMOP line.

Intriguingly, the occupation of site 1, with almost no hafnium, does not fit into this picture. Here, the bonding arguments are overruled by structural restrictions. Site 1 is too small to accommodate more than marginal amounts of hafnium. In the case of the ternary compound $Nb_{6.9}Ta_{14.1}S_8$, the average site volumes are not important to the distribution of the two different metals because they have effectively the same radii. But, for $Hf_{7.5}Ti_{13.5}S_8$, the metal radii are different (Hf 1.58 Å, Ti 1.46 Å; both 12-coordinate). Polyhedral volumes[31] for the sites and average distances for the structurally established phases are listed in Table 2, which shows that site 1 is the smallest site for all three phases. Comparison with the average distances and site volumes of the elemental metals shows clearly that site 1 is too small to accumulate hafnium. The calculated volume of site 1 in $Hf_{7.5}Ti_{13.5}S_8$ is 55.6 $Å^3$, whereas the required volume of one hafnium atom in the hexagonal closed-packed metal is 74.4 $Å^3$. Furthermore, the volumes of sites 2 and 4 are slightly smaller than the required volume of hafnium. Thus, the size requirement also puts more titanium on these sites than expected from the TMOP argument. This argument also works nicely for site 5, which again is slightly smaller than the elemental hafnium volume but has a rather large positive charge. Here the two driving forces are working against each other, resulting in an occupation slightly larger than would be expected from the TMOP argument but much less than would be expected on the basis of the electronegativity/charge argument.

Concluding Remarks

Although the occupation of metal−metal bonding levels in the $M_{21}S_8$ and $(M,M')_{21}S_8$ type phases is optimized for group 5 metals, a smaller amount of electrons resulting from the occupation of the metal sites by group 4 element atoms still gives an electronic bonding picture that suggests a stable structure. Thereby the electronic structure analysis does not contradict the existence of $(M,M')_{21}S_8$ species with mixed group 4−group 5 metals, even though such compounds have not yet been reported. The distribution of hafnium and titanium atoms on the six crystallographically independent metal sites in the ternary phase $Hf_{7.5}Ti_{13.5}S_8$ can be rationalized using metal−metal bond strength, electronegativity/charge, and site volume arguments, whereas the metal distribution in $Nb_{6.9}Ta_{14.1}S_8$ can be correlated simply with the metal−metal TMOP's of the sites.

Acknowledgment. This work was supported by the Deutsche Forschungsgemeinschaft through a postdoctoral fellowship and through a Heinrich-Hertz fellowship from the state of Northrhine Westfalia, by the DGES-Spain (Project PB96-0859), and by the Generalitat de Catalunya (Grant 1997 SGR 24). We thank H. F. Franzen (Iowa State University, Ames, IA) for helpful discussions and G. Henkel (University of Duisburg, Germany) for continuous support of this work.

IC991218T

(29) Pearson, W. B. *The Crystal Chemistry and Physics of Metals and Alloys*; Wiley-Interscience: New York, 1972; p 151.
(30) Pearson, R. G. *Inorg. Chem.* **1988**, *27*, 734−740.
(31) Finger, L. W.; Ohashi, Y. VOLCAL, a program to calculate polyhedral volumes and distortion parameters, Carnegie Institute, Washington, 1979.